INVESTIGATING THE NON-UNIQUENESS OF CRITICAL SOLID FRACTION CONSIDERING STRAIN-RATE EFFECTS

Mingze Xu[1,2], Zixin Zhang[1,2], Xin Huang[1,2]*, Kevin J. Hanley[3]

[1]Department of Geotechnical Engineering, Tongji University, Shanghai 200092, China

[2]State Key Laboratory of Geotechnical Engineering, Ministry of Education, Tongji University, Shanghai 200092, China

[3]School of Engineering, Institute for Infrastructure and Environment, The University of Edinburgh, Edinburgh EH9 3JL, United Kingdom

Corresponding author: xhuang@tongji.edu.cn

Keywords strain-rate dependency, jamming transition, force transmission network

Abstract It is well documented in the literature that the critical solid fraction (ϕ_J) which marks the transition between the solid and liquid phases in the jamming diagram is influenced by a number of factors. So far, no satisfactory explanation has been provided for the physical origin of the non-uniqueness of ϕ_J. In this study, the dependency of ϕ_J on strain rate is examined through DEM simulations considering a frictionless polydisperse granular material. It is shown that as the compression rate increases, the major force transmission network contains fewer mechanically stable particles which form a less stable force transmission network. Higher compression rates cause the granular assembly to jam at a lower solid fraction. These force transmission networks, however, are fragile and disintegrate quickly upon relaxation.

1 Introduction

Jamming is a broad concept that is related to a variety of phenomena in our daily lives: traffic may become jammed on busy roads; powders may get clogged when transported through pipes; honey may jam in winter due to a drop of temperature [1]. Jamming is also an important physical concept within granular media that distinguishes the solid phase from the liquid phase: a concept which has been extensively investigated in the past few decades.

A jammed particulate system can sustain external forces without deforming irreversibly, whereas an unjammed particulate system may flow subjected to even subtle external disturbance [2]. The transition of particulate systems from fluid-like to solid-like is called the jamming transition. The factors which influence the jamming transition of granular media can be classified into three categories: the structure, dynamical characteristics and thermodynamics [3]. Temperature was thought to be the only factor that influences the transition process until Liu and Nagel [1] pointed out that shear could also lead to a change of packing density, thereby causing a particulate system to jam. Based on this concept, they proposed a jamming diagram which defines jamming and unjamming zones in the temperature–shear stress–solid fraction space. Various interpretations of the Liu-Nagel diagram were developed by succeeding researchers [2,4].

These interpretations share a common key concept: the critical solid fraction or jamming

density, ϕ_J. A granular system can jam without external disturbance when its solid fraction is above ϕ_J. A granular system may unjam and flow when its solid fraction is below ϕ_J. Factors that may influence ϕ_J include loading rate, particle size distribution, particle shape, particle compressibility, friction and the stress path [4-7]. Contradictory observations have been reported regarding the dependency of ϕ_J on the loading rate. Hartley and Behringer [8] carried out a Couette shear experiment on assemblies of photoelastic disks and found a logarithmic correlation between the internal stresses and shearing rate. However, when they changed the loading mode from shearing to isotropic compression, they found no rate dependency of internal stresses on the loading rate. Zhang and Makse [9] used molecular dynamics simulations to find that different compression rates resulted in different values of ϕ_J. Mari et al. [10] compared jamming transition with glass transition and found that both showed a clear compression rate dependency, i.e., ϕ_J increases with decreasing compression rate. Similar observations were made by Donev et al. [11] and Speedy [12]. Vagberg et al. [13] found that isotropic compression can result in a large range of ϕ_J related to the compression rate and initial configuration. They showed that the influence of initial state persists even at an extremely slow compression rate. Vagberg et al. [13] found that shearing can only yield a small range of ϕ_J compared with isotropic compression, and at infinitesimally slow shearing rates there exists a well-defined value of critical solid fraction ϕ_J^{QS} that is independent of initial configuration. Otsuki and Hayakawa [14] repeated the shearing and relaxation process in their numerical simulations and found that the hysteresis loops formed are independent of the shearing rate. However, to the best of our knowledge, no prior study has satisfactorily explained the fundamental mechanisms underlying the strain-rate dependency of ϕ_J.

In this study, DEM simulations are conducted under periodic boundary conditions at a variety of compression rates. Microscopic analyses are conducted to investigate the particle-scale mechanism underlying the influence of strain rate on the critical solid fraction.

2 Numerical model

The simulations were run using the open-source LAMMPS code (Plimpton, 1995). A uniform strain rate field (affine transformation) is imposed on all particles confined within periodic boundaries. 20186 non-contacting frictionless spherical particles were generated within a cubic periodic cell at an initial solid fraction (ϕ_0) of 0.5. The particle size distribution follows that of Toyoura sand (Figure 1) which is polydisperse with a size ratio between the largest and the smallest particles (r_{max}/r_{min}) of 3.55. The particle density was 2650 kg/m^3 without consideration of gravity. A linear elastic model was adopted with a normal contact stiffness (k_n) of 1×10^8 N/m and a tangential contact stiffness (k_s) of 6.67×10^7 N/m. The sample was isotropically compressed at eight different compression rates (v) ranging from 0.025 m/s to 25 m/s until a jammed state was reached. Simulations were labelled PB-1 to PB-8 for compression rates of 0.025, 0.25, 2.5, 5, 10, 15, 20 or 25 m/s, respectively. The sample was firstly compressed until the solid fraction ϕ=0.63, and was then relaxed until a nearly non-contacting condition was reached, after which the sample was compressed again at the selected compression rates until the jamming state was reached.

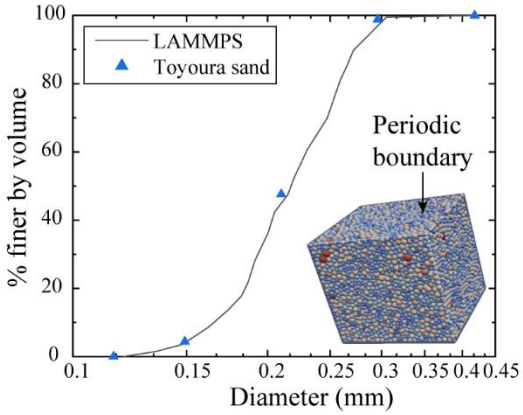

Figure 1 Comparing the particle size distributions of the DEM samples and real Toyoura sand and inset illustration showing the numerical model setup

3 Determination of critical solid fraction

3.1 Correlation between stress and solid fraction

For a DEM simulation, the global average stress tensor $\bar{\sigma}$ can be calculated as:

$$\bar{\boldsymbol{\sigma}}=\frac{1}{V}\sum_{p\in V}V^{p}*\sigma_{ij}^{p}+\frac{1}{2V}\sum_{p\in V}m^{p}v_{i}^{p}v_{j}^{p} \tag{1}$$

in which V and $\mathrm{V^p}$ are the sample volume and particle volume, respectively, σ_{ij}^{p} is the stress tensor for an individual particle of mass m^p and velocity v^p. The two terms on the right of Eq. 1 are the Cauchy and Reynolds stress tensors, respectively. Although the compression rate is relatively large in some simulations, the contribution of Reynolds stress to the overall mean stress is small (the largest contribution is 0.65% for PB-8). The isotropic mean stress P is:

$$P=tr(\bar{\boldsymbol{\sigma}})/3 \tag{2}$$

Following [7], the confining pressure P is normalized by $2\langle r\rangle/k_n$ to get a dimensionless pressure p where $\langle r\rangle$ is the mean particle radius of $2.5\times10^{-4}\,\mathrm{m}$.

The development of dimensionless pressure p during isotropic compression is shown in Figure 2. As the compression rate v increases from 0.025 m/s to 25 m/s, p becomes larger at the same solid fraction. The solid fraction corresponding to the first observance of non-zero p cannot be treated as a jamming transition point, as it has been noted both experimentally [15] and numerically [7] that this point does not exactly match the one determined from the coordination number.

3.2 Correlation between contact characteristics and solid fraction

The coordination number C^r (Eq. 3) includes the rattlers that make no contribution to force transmission. In order to eliminate the influence of the rattlers, the corrected coordination number C^* [16] is used here to quantify the mechanically stable contacts.

$$C^r = \frac{M}{N} \tag{3}$$

$$C^* = \frac{M_4}{N_4} \tag{4}$$

M is twice the total number of contacts, N is the total number of particles, M_4 is the total number of contacts owned by the N_4 mechanically stable particles which have at least 4 contacts. Figure 3 shows C^* plotted against solid fraction with different compression rates v. C^* is initially smallest for simulations with high v but the rate of increase of C^* for high v simulations is faster with increasing solid fraction than simulations with a smaller compression rate. Theoretically, in 3D problems the minimum value of C^* is 4 (the starting value on Figure 3).

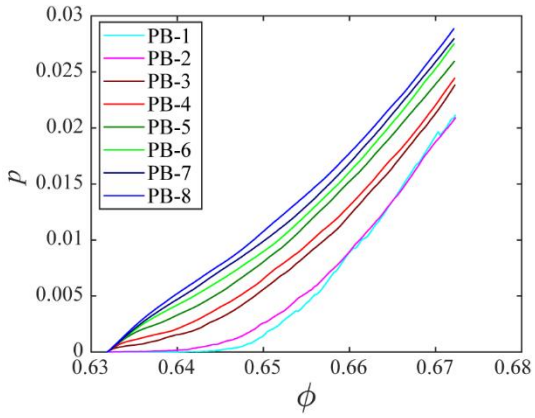

Figure 2 Variation of dimensionless p with ϕ

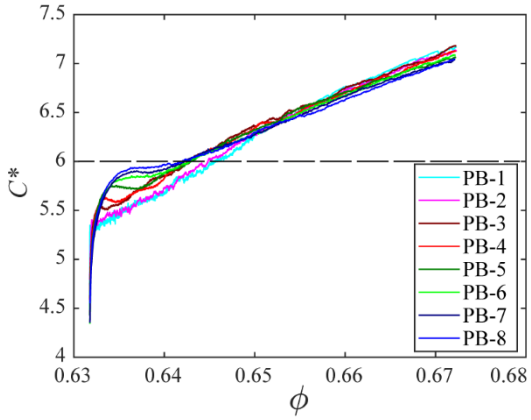

Figure 3 Variation of C^* with ϕ

Theoretically, the isostatic threshold of C^* is 6 for frictionless particles. We adopt this as the main criterion to analyze whether or not the sample reaches the isostatic state (jamming state). The value of ϕ_J is extracted from Figure 3, which corresponds to the jamming state (C^*=6) at different compression rates. As shown in Figure 4, ϕ_J decreases with increasing v.

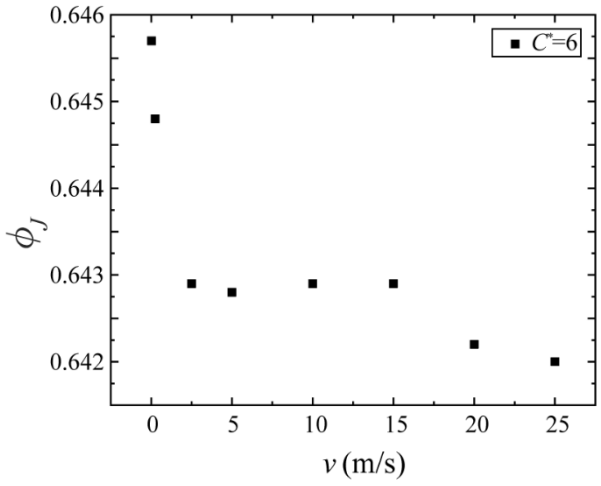

Figure 4 Variation of critical solid fraction with compression rate

After the jamming transition point, C^* follows a power-law distribution [15], i.e.,

$(C^* - C_J^*) \propto (\phi - \phi_J)^{\beta}$ with C_J^*=6 (Figure 5). The β value depends not only on ϕ_J but also on the particle size distribution: 0.8185≤ β ≤0.9947 in our simulations which is a larger range than in [15]. The relationship between β and v is plotted in the inset of Figure 5. In general, with increasing compression rate, β increases (PB-5 is the sole exception).

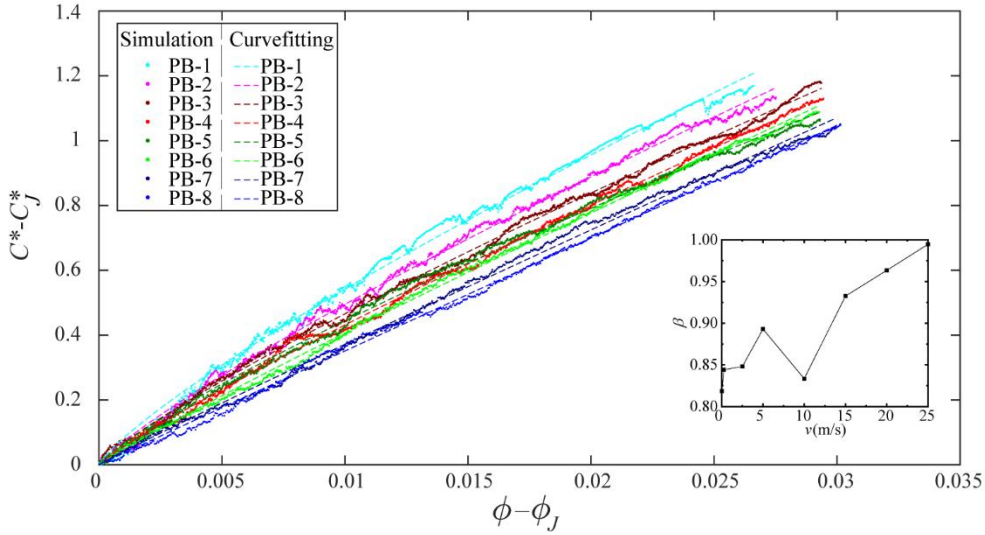

Figure 5 Curve fitting of $C^* - C_J^*$ against $\phi - \phi_J$

4 Explanation for the strain rate dependency

As observed in Section 3, the sample compressed at a higher strain rate reaches the jammed state earlier with a smaller critical solid fraction. In order to explain this phenomenon, the stability and statistical features of the force transmission network are analyzed in this section.

Figure 6 shows the distribution of particles' connectivity. In general, the sample loaded by a slower compression rate has a higher proportion of particles with connectivity ≥ 4 (Figure 6). It means that when the sample is isotropically compressed at a slower strain rate, the force transmission network contains more mechanically stable particles and should be more stable than that of samples isotropically compressed at a larger strain rate.

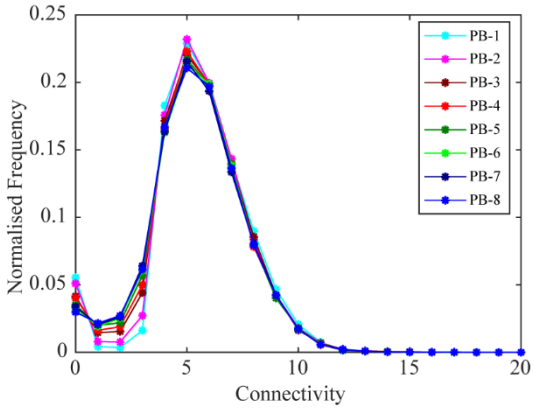

Figure 6 Distribution of particle connectivity

The contribution of the largest cluster to the normalized overall mean stress p is calculated at the jamming transition state (Figure 7). Identification of a cluster started from searching the neighbor list of a single particle. The search procedure proceeded recursively for all the identified particles having at least 4 contacting particles according to the sequence of neighbors given in the contact list until all of the particles comprising the cluster had been identified. Other clusters could be identified following the same procedure by starting from particles not already included in a cluster. The cluster having the most particles is taken as the largest force transmission network [17]. The contribution of the largest cluster to overall mean stress P can be calculated using Eq. 1 by considering those particles comprising the largest cluster only. As Figure 7 shows, the contribution of the largest cluster to overall mean stress P decreases with increasing compression rate. When the sample is isotropically compressed at a slower strain rate, the largest cluster contains more mechanically stable particles and thus sustains a larger proportion of external force, in line with Figure 6.

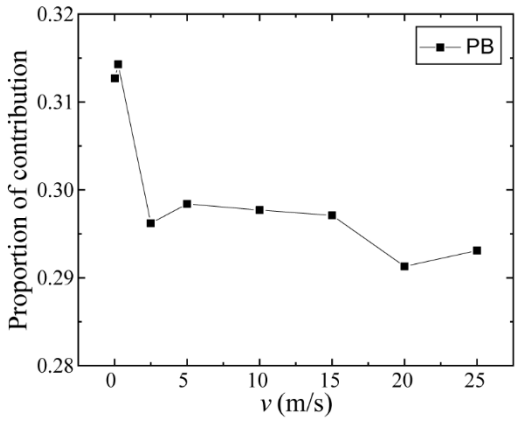

Figure 7 Contributions of largest clusters to the overall mean stress P

The stability of the force transmission network can also be inferred from its temporal contact alterations. The samples were relaxed for 100000 timesteps without change of the boundary positions to study the alteration of stresses and contacts. The dimensionless p is plotted against timestep during relaxation as shown in Figure 8. The faster v is, the larger the initial p is and the more quickly p drops. This tendency implies that, although the faster compression rate results in a larger p at the jamming state, the force transmission network is less stable compared with that at a slower compression rate. Figure 9 shows the change in the proportion of mutual contacts (contacts persisting from the beginning of relaxation to the recording timestep during the relaxation process). Note that a negligible fraction of contacts may re-form and hence be included on Figure 9. With the decrease of v, there are more persistent contacts during the relaxation period, which means that the force transmission networks are more stable at a slower compression rate than at a faster rate.

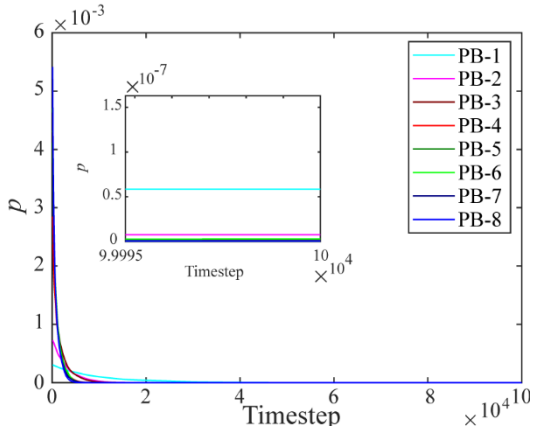

Figure 8 Dimensionless p during relaxation at the jamming transition state

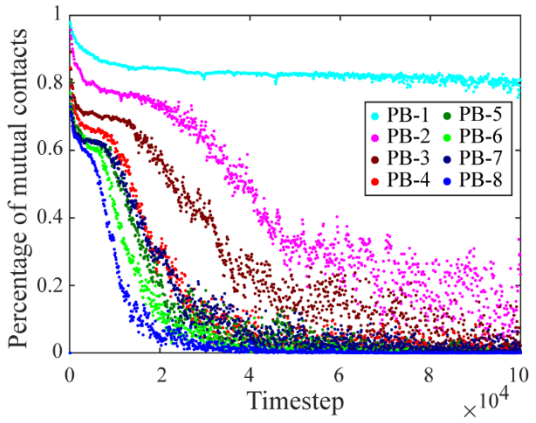

Figure 9 Contact comparison during relaxation at the jamming transition state

The results of particle connectivity, contributions of the largest contact force transmission network to overall mean stress and contact duration confirm that the stability and homogeneity of the force transmission network is the key to the strain-rate-dependency phenomenon. A faster compression rate results in a smaller critical solid fraction with a less stable force transmission network. The resultant jamming state under higher compression rates is not truly isostatic compared with that resulting from a slower compression rate.

5 Conclusion

The non-uniqueness of the critical solid fraction at the jamming state considering the strain rate effects have been systematically studied in this paper. The relationships between the dimensionless confining pressure p, the corrected coordination number C^*, critical solid fraction ϕ_J and strain rate v were analyzed. Special attention was paid to the temporal changes and stability of the force transmission networks, which are key to explain the strain-rate dependency.

In the simulations, the external forces are more concentrated in strong contacts and the force transmission network is temporal and more variable as the compression rate increases. This leads to a less stable force transmission network which causes the sample to jam at a smaller critical solid fraction in simulations with higher compression rates.

References

[1] Liu, A. J., Nagel, S. R. (1998). Nonlinear dynamics jamming is not just cool any more. Nature, 396(6706), 21-22.

[2] Bi, D., Zhang, J., Chakraborty, B., Behringer, R. P. (2011). Jamming by shear. Nature, 480(7377), 355-358.

[3] Liu, A. J., Nagel, S. R. (2010). Granular and jammed materials. Soft Matter, 6(13), 2869-2870.

[4] Ciamarra, M. P., Pastore, R., Nicodemi, M., Coniglio, A. (2011). Jamming phase diagram for frictional particles. Physical Review E, 84(4), 041308.

[5] Liu, A. J., Nagel, S. R. (2010). The jamming transition and the marginally jammed solid. Annual Review of Condensed Matter Physics, 1(1), 347-369.

[6] Vinutha, H. A., & Sastry, S. (2016). Disentangling the role of structure and friction in shear jamming. Nature Phys, 12, 578-583.

[7] Kumar, N., Luding, S. (2016). Memory of jamming–multiscale models for soft and granular matter. Granular Matter, 18(3), 58.

[8] Hartley, R. R., Behringer, R. P. (2003). Logarithmic rate dependence of force networks in sheared granular materials. Nature, 421(6926), 928-931.

[9] Zhang, H. P., Makse, H. A. (2005). Jamming transition in emulsions and granular materials. Physical Review E, 72(1 Pt 1), 011301.

[10] Mari R., Krzakala F., Kurchan J. (2009) Jamming versus Glass Transitions. Physical Review Letters, 103(2), 025701.

[11] Donev, A., Stillinger, F. H., & Torquato, S. (2006). Do binary hard disks exhibit an ideal glass transition? Physical Review Letters, 96(22), 225502.

[12] Speedy R. J. (1994). On the reproducibility of glasses. The Journal of Chemical Physics, 100(9), 6684.

[13] Vagberg, D., Olsson, P., Teitel, S. (2011). Glassiness, rigidity, and jamming of frictionless soft core disks. Physical Review E, 83(3), 031307.

[14] Otsuki, M., Hayakawa, H. (2011). Critical scaling near jamming transition for frictional granular particles. Physical Review E, 83(1), 051301.

[15] Majmudar, T. S., Sperl, M., Luding, S., Behringer, R. P. (2007). Jamming transition in granular systems. Physical Review Letters, 98(5), 058001.

[16] Imole, O. I., Kumar, N., Magnanimo, V., Luding, S. (2013). Hydrostatic and shear behavior of frictionless granular assemblies under different deformation conditions. Powder and particle, 30(30), 84-108.

[17] Huang, X., Hanley, K.J., Zhang Z.X., Kwok, C.Y. (2019). Structure degradation of sands during cyclic liquefaction: Insight from DEM simulations, Computers and Geotechnics, 114, 103139.